JOURNAL OF AIRCRAFT
Vol. 37, No. 2, March–April 2000

Study of Icing Effects on Performance and Controllability of an Accident Aircraft

A. Reehorst,* J. Chung,† M. Potapczuk,‡ and Y. Choo‡
NASA John H. Glenn Research Center at Lewis Field, Cleveland, Ohio 44135

The activities at NASA John H. Glenn Research Center at Lewis Field in support of a National Transportation Safety Board accident investigation are described. An icing research tunnel (IRT) test was conducted in January 1998. Most conditions for the test were based on raw and derived data from the flight data recorder recovered from the accident and on the current understanding of the meteorological conditions near the accident. Using a two-dimensional Navier–Stokes code, the flowfield and resultant lift and drag were calculated for the wing section with various ice shapes accreted in the IRT test. Before the final calculations could be performed extensive examinations of geometry smoothing and turbulence modeling were conducted. The most significant finding of this effort is that several of the 5-min ice accretions generated in the IRT were found by the Navier–Stokes analysis to produce severe lift and drag degradation. The information generated suggests a possible scenario for the kind of control upset recorded in the accident. Secondary findings were that the ice shapes accreted in the IRT were mostly limited to the protected pneumatic boot region of the wing and that during testing activation of the pneumatic boots cleared most of the ice.

Introduction

IN early 1997, a twin-engine commuter aircraft (Fig. 1) crashed during a rapid descent after an uncommanded roll excursion. There were no survivors. The ground impact forces and postaccident fire destroyed the aircraft. Instrument meteorological conditions prevailed at the time of the accident.[1] During the investigation, the National Transportation Safety Board (NTSB) contacted the Icing Branch at NASA John H. Glenn Research Center at Lewis Field. The NTSB requested NASA's participation because ice contamination was suspected as being a factor. NASA offered to pursue a study that included experimental and computational elements to identify the broad nature of possible ice contamination and the likely associated performance degradation.

Project Methodology

The primary goal of the NASA activity supporting the NTSB investigation was to attempt to identify a mechanism explaining the stability and control upset that preceded the accident. The methodology that was adopted to satisfy this goal was a multistep process that included both computational and experimental tasks.

Ice shapes were defined by a test in the Icing Research Tunnel (IRT). Ice shapes were defined experimentally instead computationally due to uncertainties in current ice accretion prediction codes very near freezing temperatures, as was the case here. The complex movement of liquid water on the airfoil prior to its freezing is currently modeled by simplified relationships in all ice accretion codes. Because of this limitation and other assumptions required by ice accretion codes, the ice shapes predicted at temperatures near freezing are not always as accurate as those predicted for lower temperatures.

The contaminated airfoil geometries measured during the IRT test were then analyzed with a two-dimensional Navier–Stokes code to predict their degraded aeroperformance. Because of the time constraints of this project, the icing wind-tunnel test concentrated on measuring the ice accretion shapes, with all aerodynamic analysis performed computationally.

To verify that the two-dimensional analysis was producing realistic results (that no significant three-dimensional flow effects were present), a limited three-dimensional Navier–Stokes analysis was conducted. The three-dimensional analysis was focused on assuring that no significant spanwise flow was present that would invalidate the chordwise flow assumption required by the two-dimensional Navier–Stokes analysis.

IRT Test

The IRT is a closed-loop atmospheric tunnel with a test section that is 6 ft high, 9 ft wide, and 20 ft long. It is equipped to support testing at airspeeds from 50 to 430 mph in a temperature and water-droplet environment that simulates natural icing conditions.[2] Temperature is controllable between −20 and +33°F. Clouds can be produced in a controlled manner with droplet mean volumetric diameter (MVD) between 9.5 and 270 μm.

For this test an existing model was utilized. The model was a modified piece of wing from the subject aircraft. The wing section of the accident aircraft is a NACA 23012 airfoil at the tip and a modified NACA 23018 airfoil at the root. The model had a 6-ft span centered on the inboard region of the aileron. It was mounted vertically in the IRT (Fig. 2). The wing had a modified trailing edge and pneumatic boot. The trailing edge was faired behind the aft spar to avoid the mechanical complexity of the aileron. The pneumatic boot was modified for its original test to allow the incorporation of thermal measurements. This feature was not utilized for this subject testing; however, the modification resulted in the boot material extending farther aft on the lower surface than a production boot for this wing. Note that the active region of this boot was similar to that of the production aircraft. The extended boot material acted as an enhanced ice accretion location that is evident when reviewing the test ice shape tracings. Except for the cases when the pneumatic boot was activated, the manufacturers recommended level of vacuum was applied to the boot throughout the testing to prevent autoinflation. To ensure that the air temperature in the test section was accurate at the desired near-freezing condition, an auxiliary temperature probe was mounted near the model as seen in Fig. 2. Based on this extra probe and the standard wind-tunnel temperature system, the temperatures during this test were held to the planned conditions within the measurement accuracies of the temperature instrumentation.

Presented as Paper 99-0374 at the AIAA 27th Aerospace Sciences Meeting, Reno, NV, 11–14 January 1999; received 5 August 1999; revision received 29 October 1999; accepted for publication 31 October 1999.

*Aerospace Engineer, Icing Branch.
†Senior Research Associate, Institute for Computational Mechanics in Propulsion.
‡Aerospace Engineer, Icing Branch.

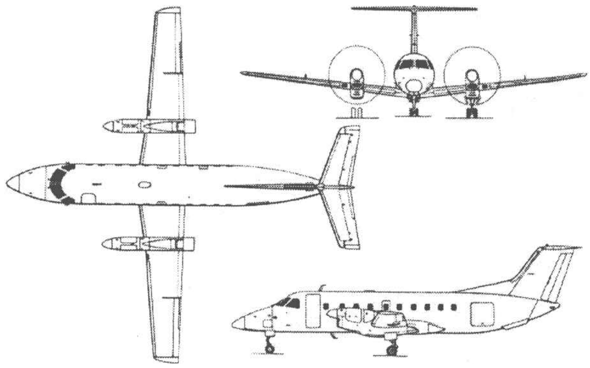

Fig. 1 Twin-engine commuter aircraft.

Fig. 2 Model installed in IRT.

Test Environment Conditions

Based on the findings of the investigation's meteorological team,[3] the accretion time, the maximum liquid water content (LWC), and the cloud droplet's MVD were estimated for this test. The accretion time was estimated at 5 min. This was the length of time required by the accident aircraft to transit an area of low reflectivity evident on regional weather radar. This time also agrees with estimates based on a measurable drag increase calculated by the investigation's performance team from flight data recorder (FDR) information.[4] The maximum LWC was estimated to be 0.8 g/m^3 based on microwave radiometer measurements of the same airmass following the accident. The maximum MVD of the cloud droplets was estimated to be no greater than 70–80 μm. This droplet-sizing estimate was considered reasonable because the aircraft was known to have been in the clouds, and droplets larger than that are normally associated with below-cloud drizzle.

The remaining test parameters were defined based on a combination of the accident meteorological data and the FDR information. The times that defined the assumed icing period from the meteorological report were used to access the pertinent information from the FDR. Representative airspeed, aircraft angle of attack, and air temperature values were calculated by averaging over the assumed ice accretion period (total air temperature was derived from static air temperature measurements and corrected for altitude and airspeed, and wing angle of attack was calculated by adding the wing incident angle to the aircraft body angle of attack).

The combination of the assumed cloud conditions and the measured flight environment data was used to define the IRT test matrix (Table 1). Four conditions were considered the baseline series in the matrix. Because of uncertainties in the FDR measured values of angle of attack and temperature, additional series were added to the matrix that examined higher and lower angle of attack than the baseline value and higher and lower temperatures than that baseline value. An additional series with longer accretion time was also added because the ice accretion time was inferred information and not directly measured. A series of supercooled large droplet (SLD) conditions was added during the testing at the request of the NTSB to ensure the completeness of the database. To add to the level of confidence in the IRT results, all primary conditions were repeated at least once.

Test Procedure

The IRT test was conducted over two weeks in January 1998. The conditions described in Table 1 were used for this test, and the most significant conditions were repeated at least once. The normal process used during this test was to cool the IRT to the desired temperature and set the airspeed. When the temperature and airspeed were stable at the desired test conditions, the spray was activated for the length of time at air and water pressures defined by the test matrix to simulate a natural icing cloud. When the spray was shut off, several wake survey probe traverses were made behind the model. These wake probe traverses were used to calculate an uncorrected tunnel centerline section drag. Because of project time constraints, further correction, analysis, and comparisons of these data have not been completed. Following the wake probe traverses, the tunnel fan was stopped so that test personnel could enter the test section. On entering the test section, the test engineers would first photograph the model. Both digital and film cameras were utilized for this test, with the film photographs typically being used for close-up detailed shots and the digital photographs for overview shots (Figs. 3 and 4). When the photographs were completed, the leading-edge ice accretion was sliced with a hot knife, then traced

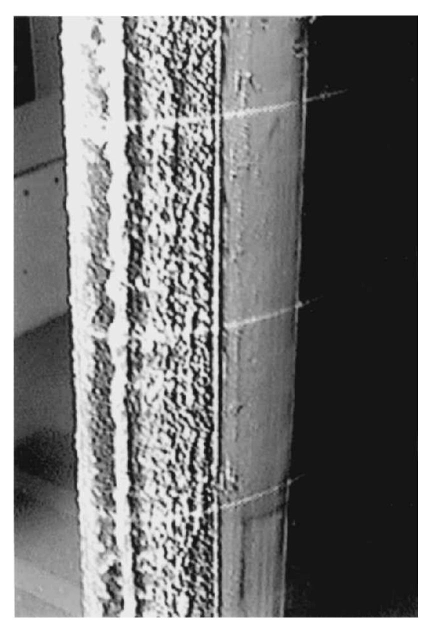

Fig. 3 Digital photograph of model with ice accretion.

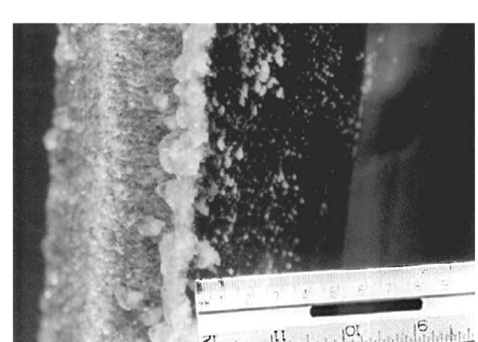

Fig. 4 Close-up film photograph of ice accretion.

Table 1 Test matrix

Matrix number	A/S, kn	Total temperature, °F	Angle of attack, deg	LWC, g/m^3	MVD, μm	Time, min	Comment
1	172	——	——	——	——	——	Clean wake run
2	172	30	5	0.8	20	5	Baseline series
3	172	30	5	0.8	40	5	Baseline series
4	172	30	5	0.52	40	5	Baseline series
5	172	30	5	0.58	70	5	Baseline series
6	172	30	7	0.8	20	5	Higher AOA series
7	172	30	7	0.8	40	5	Higher AOA series
8	172	30	7	0.52	40	5	Higher AOA series
9	172	30	7	0.58	70	5	Higher AOA series
10	172	——	——	——	——	——	Clean wake run
11	172	——	——	——	——	——	Clean wake run
12	172	30	3	0.8	20	5	Lower AOA series
13	172	30	3	0.8	40	5	Lower AOA series
14	172	30	3	0.52	40	5	Lower AOA series
15	172	30	3	0.58	70	5	Lower AOA series
16	172	31	5	0.8	20	5	Higher temperature series
17	172	31	5	0.8	40	5	Higher temperature series
18	172	31	5	0.52	40	5	Higher temperature series
19	172	31	5	0.58	70	5	Higher temperature series
20	172	——	——	——	——	——	Clean wake run
21	172	——	——	——	——	——	Clean wake run
22	172	28	5	0.8	20	5	Lower temperature series
23	172	28	5	0.8	40	5	Lower temperature series
24	172	28	5	0.52	40	5	Lower temperature series
25	172	28	5	0.58	70	5	Lower temperature series
26	172	26	5	0.8	20	5	Lower temperature series II
27	172	26	5	0.8	40	5	Lower temperature series II
28	172	26	5	0.52	40	5	Lower temperature series II
29	172	26	5	0.58	70	5	Lower temperature series II
30	172	——	——	——	——	——	Clean wake run
31	172	——	——	——	——	——	Clean wake run
32	172	30	5	0.8	20	10	Longer time series
33	172	30	5	0.8	40	10	Longer time series
34	172	30	5	0.52	40	10	Longer time series
35	172	30	5	0.58	70	10	Longer time series
36	172	——	——	——	——	——	Clean wake run
37	172	30	5	0.6	100	5	Additional SLD series
38	172	30	5	0.6	120	5	Additional SLD series
39	172	30	5	0.85	175	5	Additional SLD series
40	172	30	5	0.85	270	5	Additional SLD series
41	172	28	5	0.6	100	5	Additional SLD series
42	172	30	3	0.6	100	5	Additional SLD series
43	172	30	7	0.6	100	5	Additional SLD series

Fig. 5 Ice tracing technique.

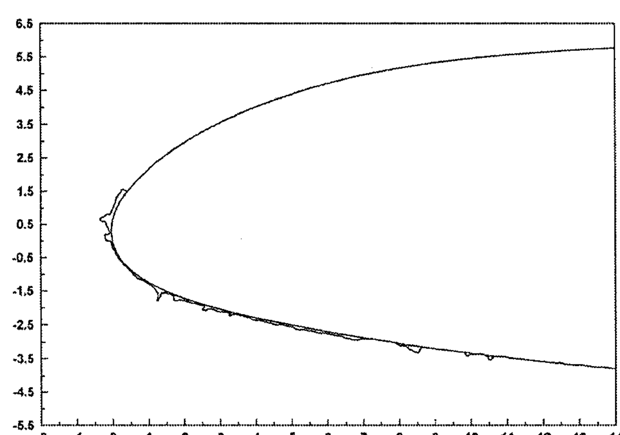

Fig. 6 Baseline condition, matrix 2 tracing.

onto a cardboard template (Fig. 5). These tracings were made at 30, 36, and 42 in. from the wind-tunnel floor (the 36-in. location is the vertical center of the test section). The ice shapes originally traced onto cardboard are then later digitized and stored electronically. All tracings presented here are digitized data (Fig. 6). Three channels of video were also recorded for each ice accretion. The video cameras captured upper and lower leading-edge views along with a broad model view. The video signals were recorded to Super VHS (SVHS) format tapes.

Resultant Ice Accretions

Based on visual examination, repeatability was good for all cases, with the volume of ice, impingement limits, and horn or ridge location closely matched for repeat cases. The majority of the ice shapes accreted during this test fell into two categories. The first was a thin ice shape with a rough surface made up of small bumps of varying size and sharpness (Fig. 6). The second category of ice shape had the same general volume of ice with similar roughness elements as the first category, but also a prominent ridge approximately 0.5 in. high.

The baseline series (see Table 1) resulted in thin ice accretions with distributed roughness and no ridge formation for all four of the series conditions (Figs. 6–9).

As the angle of attack was increased from 5 to 7 deg, the ice shapes were shifted toward the lower surface as would be expected (Fig. 10). Because the upper impingement limit moved forward, the overall ice thickness of these shapes was somewhat greater than that seen in the baseline series.

At the lower angle of attack (3 deg instead of the baseline 5 deg), no significant difference from the baseline series was evident.

The higher temperature series cases (31°F total temperature instead of 30°F) did not appear significantly different than the baseline series, but may have had a very slight decrease in the total volume of ice accreted.

However, the lower temperature series (at 28°F total temperature instead of 30°F) produced slightly more total ice volume than the baselines series and, more importantly, started to exhibit some ridge formation for the 40- and 70-μm MVD cases (Figs. 11 and 12).

The second lower temperature series (at 26°F total temperature instead of 30°F) exhibited an ice ridge for all four conditions

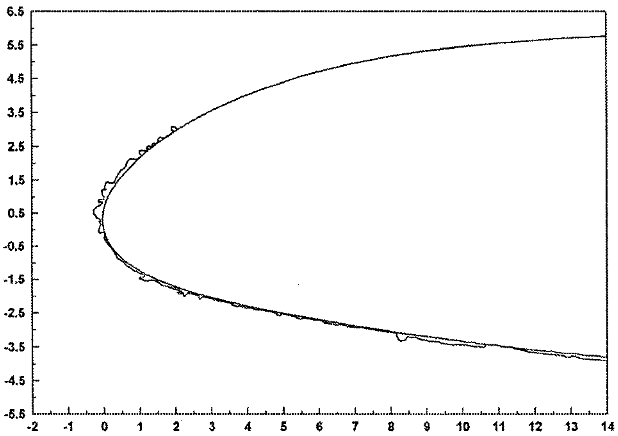

Fig. 7 Baseline condition, matrix 3 tracing.

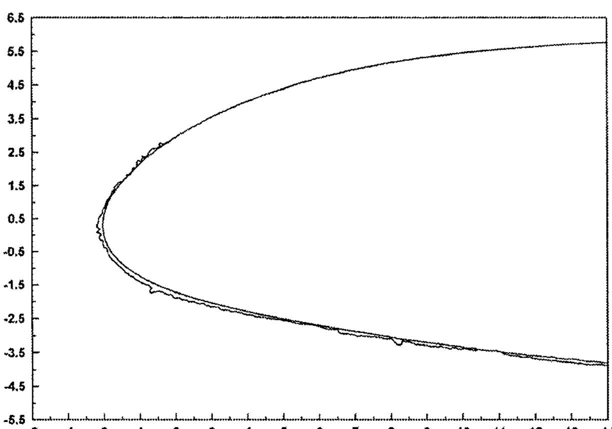

Fig. 8 Baseline condition, matrix 4 tracing.

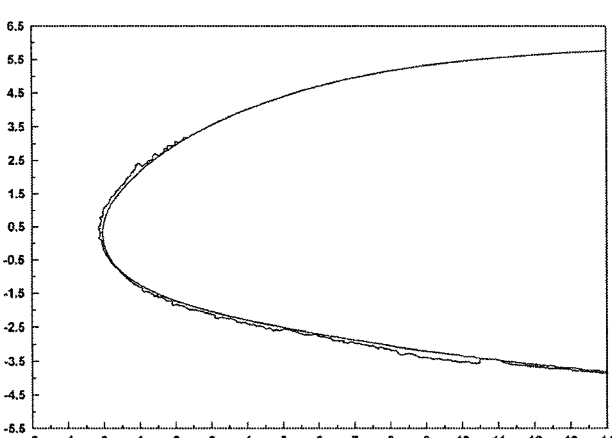

Fig. 9 Baseline condition, matrix 5 tracing.

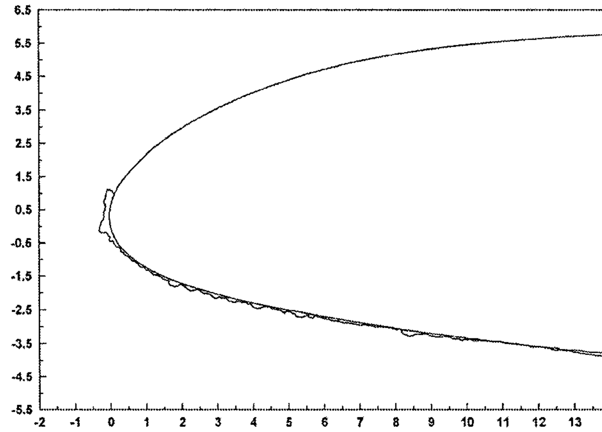

Fig. 10 Higher angle-of-attack condition, matrix 6 tracing.

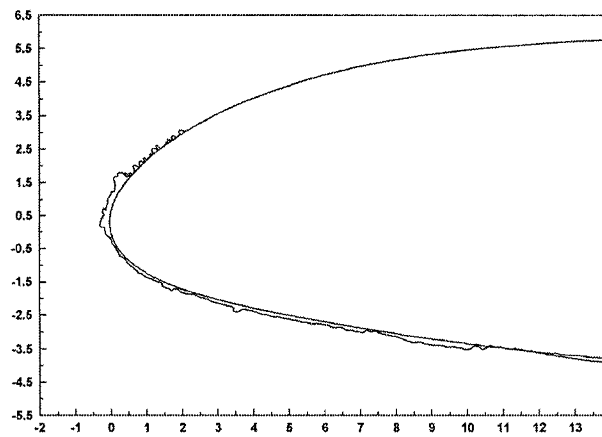

Fig. 11 Lower temperature condition, matrix 23 tracing.

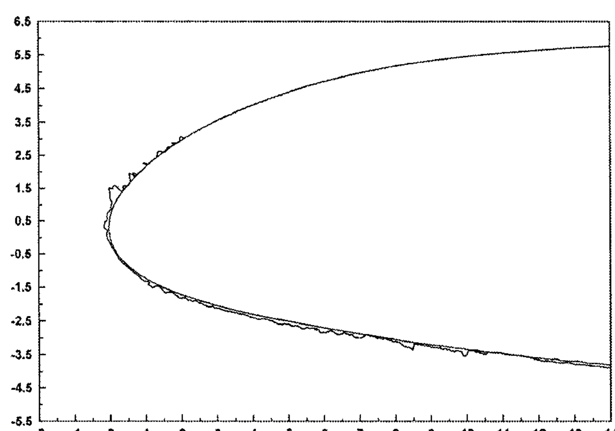

Fig. 12 Lower temperature condition, matrix 25 tracing.

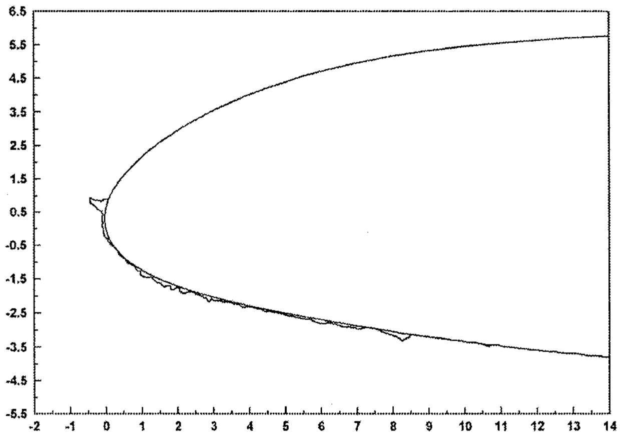

Fig. 13 Second lower temperature condition, matrix 26 tracing.

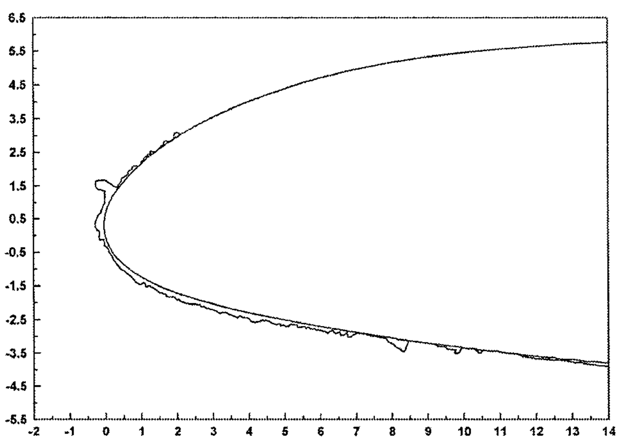

Fig. 14 Second lower temperature condition, matrix 27 tracing.

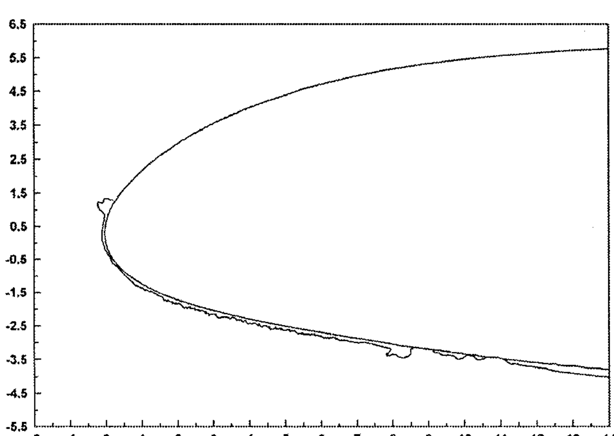

Fig. 15 Second lower temperature condition, matrix 28 tracing.

(Figs. 13–16). The ridges apparent in these accretions are different from a standard horn formation in that they are surrounded by only a thin layer of ice, where a standard horn is part of a more substantial ice accretion. The ridge was most prominent for the two cases with LWC = 0.8 g/m^3 (matrices 26 and 27, Figs. 13 and 14). For the two cases with constant LWC, the ridge moved aft with increasing MVD. For the two cases with constant MVD, the ridge moved aft with increasing LWC.

In the longer time series (with an accretion time of 10 min instead of 5 min), self-shedding occurred on the upper surface in matrix 32. For the remaining cases in this series the ice mass was greater than in the baseline series, as would be expected. These shapes also exhibited a ridge formation (Fig. 17). However, these ridge formations appeared to be much more like a standard horn formation. These ice

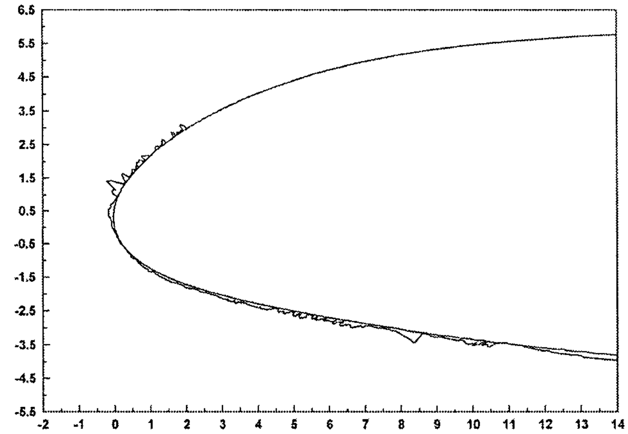

Fig. 16 Second lower temperature condition, matrix 29 tracing.

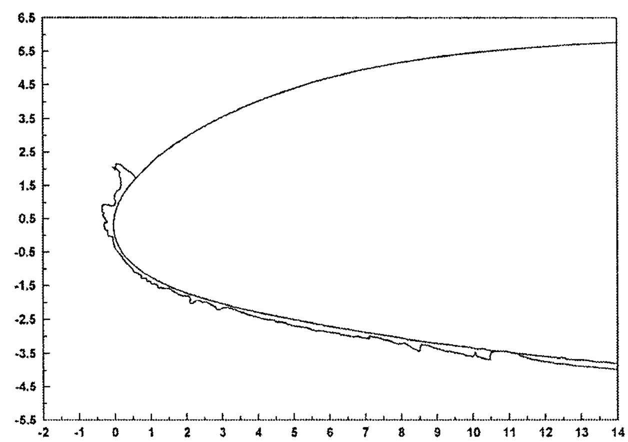

Fig. 17 Ten minute accretion condition, matrix 34 tracing.

shapes were, in general, larger and rougher than those seen in the baseline series.

The additional SLD series (which extended the MVD up to 270 μm from the baseline maximum of 70) showed no significant difference in the leading-edge ice accretion over those exhibited in the baseline series, except that the 175- and 270-μm cases self-shed.

The pneumatic boot was operated for several cases in the de-ice series. It was operated for the matrices 3, 26, and 27 conditions. Depending on the case, the pneumatic boot was either activated at sprayoff only, at 2 min into a 5-min spray, or at 2 min and at sprayoff. In all cases when the pneumatic boot was operated at the end of the icing spray, the leading-edge ice shed very well. For the two cases when the boot was activated at 2 min into a 5-min spray, in one case it prevented the development of a ridge formation, and in the other case it did not. Whether the ridge was suppressed or not was probably dependent on how well the boot cleared the ice at the 2-min activation. Note that the pneumatic boot used during this test was not a production boot, and it had never experienced the operational environment. However, no special steps were taken to enhance the boot performance, such as the application of Ice-X, and it was operated at the same pressures as a flight system. The boot performance in the de-icing tests is, therefore, considered to be broadly representative of that of a flight system.

The physics involved in the development of the ice ridges observed during this test are not well understood. It is very possible that the ridges are a result of the damming of surface runback water by ice feathers. The ridges appear to have formed at the aft edge of the primary ice accretion where ice feathers begin. Ice damming by ice feathers has been observed by close-up videography[5] and may explain this form of ice growth. More research is required into the formation of the ice ridges seen in this test and, more generally, into the movement of liquid water on developing ice accretions.

Computational Analysis

The computational analysis performed as part of this effort is described in two AIAA reports.[6,7] The computational analysis consisted of both two-dimensional and three-dimensional Navier–Stokes[8] computations. As described, the performance of the ice-contaminated wing was calculated via computational techniques instead of by experiment to complete the analysis in a timely manner for the NTSB investigation.

Four cases of the IRT ice shapes were selected for computational analysis based on their varying nature. The ice shape from test matrix condition 2 was selected because it exhibited a thin ice accretion with many small roughness elements. Matrix 3 was also selected because it exhibited larger, sharper roughness elements than did matrix 2. Matrix 9 was selected because it exhibited the roughness of matrix 2, but also had a larger accretion on the upper surface. Finally, the resultant ice shape form matrix 26 was selected because it exhibited a significant ridge formation.

For the two-dimensional calculations, a significant effort was undertaken to determine the best level of ice tracing point smoothing and optimal grid point resolution.[6,7] The calculated lift curves of the four ice shapes examined compared to that of the clean airfoil are presented in Fig. 18. As expected, when ice was added to the airfoil, the calculated lift was degraded. The matrix 2 shape had the least degradation because it had the lowest level of roughness of the shapes examined, followed by the matrix 3 shape, which had larger, rougher roughness elements. When the ice thickness increased, as in matrix 9, the lift degradation was further increased. The surprising result was the level of degradation when a ridged ice shape was examined. The major difference between the ice shape from matrix 2 and that from matrix 26 was the ice ridge. The roughness levels observed in the two cases were very close. When the ice ridge was present, a 45% reduction of maximum lift coefficient $C_{L\max}$ was predicted in comparison to the clean airfoil. Because the ridged ice shape caused the greatest lift degradation, it was selected for all further computational analysis. Note that the calculated lift degradation for the smallest accretion with rough ice and no ridge agrees well with the standard roughness results for a NACA 23012 airfoil of Abbott and vonDoenhoff.[9]

Of equal significance compared to the lift degradation caused by the ice contamination is the effect of aileron deflection for contaminated airfoils. Navier–Stokes calculations were performed for the wing in the configuration at the moment of the control upset. The moment of control upset was defined for this activity as the point

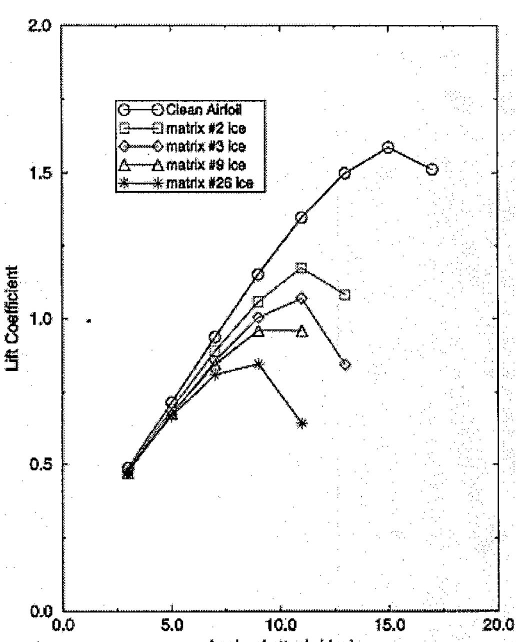

Fig. 18 Lift curves for clean airfoil and airfoil contaminated with various ice shapes.

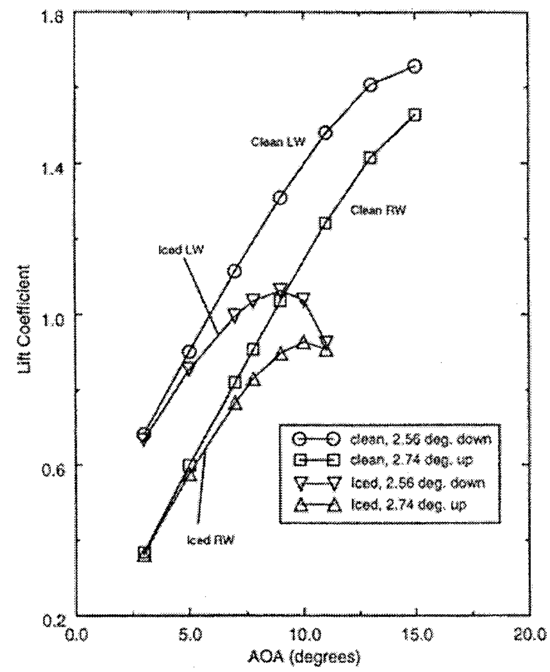

Fig. 19 Lift curves for clean airfoil and ridge ice shape contaminated airfoil with aileron deflections.

when the aircraft's roll no longer tracked the aileron input. Note that the aircraft flight variables of interest here (airspeed, angle of attack, altitude, and temperature) are different from those used to simulate the possible ice shapes in the IRT because the accretion of ice and the control upset occurred at different times and spatial positions.

When the aileron deflection effect was added to the degradation caused by the ridged ice shape, the lift curves in Fig. 19 resulted. The clean left wing (clean LW) line represents the lift curve for the airfoil with the aileron deflected down at 2.56 deg. The clean right wing (clean RW) line represents the lift curve for the airfoil with the aileron deflected up at 2.74 deg. The LW generates more lift than the RW; therefore, the aircraft will roll right. This was the intention of the pilot when these control inputs were made. However, with the ridged ice shape contamination on the wings, both the iced LW and iced RW lines show how the left and right airfoil lift curves were degraded. As angle of attack increases the differential lift decreases and at an angle of attack around 11 deg the difference in lift between the two wings goes to zero. This calculated degraded roll control authority is a possible factor explaining why the aircraft continued to roll to the left when the aileron inputs were commanding a right roll. Additional factors that may have contributed to the uncommanded roll include aircraft yaw, asymmetric power application, propeller effects, and established roll rate.

At the completion of the two-dimensional analysis a limited three-dimensional analysis was undertaken.[7,8] The LW geometry, including aileron deflection but minus engine nacelle, was applied to a three-dimensional structured grid. Developing a grid that accurately captured the wing geometry and also allowed the Navier–Stokes code to converge took a great deal of effort. To allow the convergence of the Navier–Stokes code in a timely manner the grid resolution used was relaxed. The resultant three-dimensional flowfield demonstrates a chordwise flow over the wing. The trailing-edge stall mechanism is also similar to that seen in the two-dimensional analysis; however, the stall occurred much more abruptly in three-dimensions than it did in two-dimensions. In three-dimensions the separation started right before the stall, but for two-dimensions the separation started several degrees before the stall. The angle of attack for stall in the three-dimensional analysis is also higher than that for the two-dimensional analysis. These differences may be caused by the relaxed grid resolution utilized for the three-dimensional calculations; the minimum grid spacing used for the two-dimensional calculations was $2.0 \times 10^{-6} y/c$ whereas the minimum grid spacing used for the three-dimensional calculations was $5.0 \times 10^{-6} y/c$. Although explainable, the difference between the two-dimensional and three-dimensional results does warrant further investigation. A preliminary experimental comparison has also been made with results generated by the University of Illinois at Urbana–Champaign.[10] Although the airfoil used for the experiment was different than that used for this computational activity, the ice ridged shape was similar. The experimental stall angle is greater than that predicted by the NASA two-dimensional effort, but occurs due to trailing-edge flow separation. The nature of the flow results appear to be similar to the NASA results, but, as stated before, more research will be required before the computational results can be utilized independently with complete confidence.

Summary of Significant Experimental and Computational Findings

The ice shapes accreted during the IRT test largely fell into two categories. The first was a thin ice shape with a rough surface made up of small bumps of varying size and sharpness. The second category of ice shape had the same general volume of ice with similar roughness elements as the first category, but also a prominent ridge. This ridge was approximately 0.5 in. high.

In all cases when the pneumatic boot was operated at the end of the icing spray, the leading edge ice shed very well.

Of the four ice shapes analyzed with the Navier–Stokes code, the degraded $C_{L\max}$ from the ice shape with the lowest level of roughness, matrix 2, was about 75% of the clean airfoil. The $C_{L\max}$ from the ice shape with larger, sharper roughness elements, matrix 3, was about 68% of the clean airfoil. The $C_{L\max}$ from the rough shape with more ice accretion on the upper surface of matrix 9 was about 60% of the clean airfoil, and the $C_{L\max}$ from the ice ridge case, matrix 26, was about 53% of the clean airfoil.

With the aileron effects added to the lift degradation caused by the ridged ice shape, the resultant lift curves for the LW and RW airfoils display that little or no lift difference may have been present and, therefore, roll control authority may have been significantly degraded.

Although three-dimensional computational and experimental results do not directly confirm the two-dimensional Navier–Stokes results, they do confirm the general flow characteristics and stall mechanism, and enough differences exist between the two-dimensional and three-dimensional grids and the computational and experimental geometries to account for the differences in results.

Conclusions

There are many lessons to be learned by this activity. The NASA Icing Branch has gained a significant amount of experience in measuring wind-tunnel-generated ice shapes and determining the aerodynamic performance for a contaminated wing. Along with this added knowledge have come more questions. What are the physical processes that led to the generation of the ridged ice shapes? Is there a different formation mechanism for leading-edge ridge accretions compared to the ridges that form further aft that result from SLD conditions? How do varying ridge locations and heights influence airfoil and wing performance? How well do the Navier–Stokes codes compare to experimental aeroperformance data, and how can the agreement be improved? What is the best way of using the two-dimensional and three-dimensional codes together? There is a significant amount of work that needs to be accomplished before these question are answered and before we have a good understanding and confidence in all of the methodologies.

The authors therefore recommend that the following activities be pursued:

1) Additional testing should be conducted to gain an understanding of the ice ridge formation process.

2) More analysis and testing should be conducted to understand the criticality of the ice ridge in regards to airfoil performance. This needs to include both ridge location and height.

3) A comparision should be made of the computational results from two-dimensional and three-dimensional Navier–Stokes code utilized to other Navier–Stokes codes using the same geometry and conditions.

4) Aeroperformance testing should be conducted and comparison made to the Navier–Stokes solutions.

The other lessons learned through this activity relate to the operation of aircraft in icing conditions. Based on the cockpit voice recorder from the accident aircraft, it appears that the flight crew was unaware of the potential hazard of their flight situation. Although the total ice accretion was probably quite small, the aerodynamic effects appear to have been severe. For this incident, relying on past experiences and guidelines that suggested waiting until significant accretions existed before activating the pneumatic ice protection systems may have been a fatal error. Because of the limited information recorded, we will never be completely sure of the cause of this accident and can surely never know the level of awareness and intentions of the flight crew. However, based on a review of the NASA results from this study along with the group consensus at the Joint NASA/FAA Airplane Deicing Boot Ice Bridging Workshop, November 1997, two operational suggestions become apparent:

1) Even ice accretions that may appear small and benign can be truly hazardous. Treat all icing conditions and resultant ice accretions as threats to your aircraft.

2) Unless otherwise instructed by the aircraft flight manual, activate the ice protection systems at first indication of ice accretion; do not wait until a significant accretion has formed.

References

[1] Aircraft Accident Rept., "In-Flight Icing Encounter and Uncontrolled Collision with Terrain, Comair Flight 3272, Embraer EMB-120T, N265CA, Monroe, MI, 9 Jan. 1997," NTSB DCA97MA017.

[2] Soeder, R. H., Sheldon, D. W., Andracchio, C. R., Ide, R. F., Spera, D. A., and Lalli, N. M., "NASA Lewis Icing Research Tunnel User Manual," NASA TM-107159, June 1996.

[3] "Meteorological Group Chairman's Factual Report," National Transportation Safety Board Accident DCA97MA017.

[4] "Group Chairman's Aircraft Performance Study," National Transportation Safety Board Accident DCA97MA017.

[5] Hansman, R. J., Breuer, K. S., Hazan, D., Reehorst, A., and Vargas, M., "Close-up Analysis of Aircraft Ice Accretion," AIAA Paper 93-0029, Jan. 1993; also NASA TM-105952, 1993.

[6] Chung, J., Reehorst, A., Choo, Y., and Potapczuk, M., "Effect of Airfoil Ice Shape Smoothing on the Aerodynamic Performances," AIAA Paper 98-3242, July 1998.

[7] Chung, J., Choo, Y., Reehorst, A., Potapczuk, M., and Slater, J., "Navier–Stokes Analysis of the Flowfield Characteristics of an Ice Contaminated Aircraft Wing," AIAA Paper 99-0375, Jan. 1999.

[8] Chung, J., Slater, J. W., Suresh, A., and Townsend, S., "NPARC v 3.1 User's Guide: A Companion to the NPARC v 3.0 User's Guide," NASA/TM-1999-209058, March 1999.

[9] Abbott, I. H., and vonDoenhoff, A. E., *Theory of Wing Sections*, Dover, New York, 1959, p. 499.

[10] Lee, S., Dunn, T., Gurbachi, H. M., Bragg, M. B., and Loth, E., "An Experimental and Computational Investigation of Spanwise-Step-Ice Shapes on Airfoil Aerodynamics," AIAA 98-0490, Jan. 1998.